Editors' Suggestion

Time-Dependent Multistate Switching of Topological Antiferromagnetic Order in Mn_3Sn

Gunasheel Kauwtilyaa Krishnaswamy,[1,*] Giacomo Sala,[1] Benjamin Jacot,[1] Charles-Henri Lambert,[1] Richard Schlitz,[1] Marta D. Rossell,[2] Paul Nöel,[1] and Pietro Gambardella[1]

[1] *Department of Materials, ETH Zurich, 8093 Zurich, Switzerland*

[2] *Electron Microscopy Center, Empa, Swiss Federal Laboratories for Material Science and Technology, Dübendorf, Switzerland*

(Received 10 May 2022; revised 11 July 2022; accepted 20 July 2022; published 23 August 2022)

The manipulation of antiferromagnetic order by means of spin-orbit torques opens opportunities to exploit the dynamics of antiferromagnets in spintronic devices. In this work, we investigate the current-induced switching of the magnetic octupole vector in the Weyl antiferromagnet Mn_3Sn as a function of pulse shape, magnetic field, temperature, and time. We find that the switching behavior can be either bistable or tristable depending on the temporal structure of the current pulses. Time-resolved Hall effect measurements performed during the current pulsing reveal that Mn_3Sn switching proceeds via a two-step demagnetization-remagnetization process caused by self-heating over a timescale of tens of nanoseconds followed by cooling in the presence of spin-orbit torques. Single-shot switching measurements with 50-ps temporal resolution indicate that chiral spin rotation is either damped or incoherent in polycrystalline Mn_3Sn. Our results shed light on the switching dynamics of Mn_3Sn and prove the existence of extrinsic limits on its switching speed.

DOI: 10.1103/PhysRevApplied.18.024064

I. INTRODUCTION

Electric control of magnetic order in antiferromagnets has raised prospects for realizing high-speed and high-density magnetoelectric devices using materials with zero net magnetization [1–6]. The switching of the order parameter in antiferromagnets is achieved by either injecting spin currents from an adjacent heavy metal layer or current-induced spin-orbit torques intrinsic to noncentrosymmetric crystals [7]. Electrical readout, however, is problematic because of the small magnetoresistance [8], resistive artefacts [9–11], and absence of Hall effect in most conventional antiferromagnets. This problem can be elegantly solved by turning to noncollinear antiferromagnets, which combine topologically nontrivial electronic properties with chiral magnetic order. In these systems, the broken time-reversal symmetry and large Berry curvature in momentum space give rise to strong anomalous Hall effect (AHE) [12,13] and magneto-optical responses [14–17], similar to those of ferromagnets but in the absence of significant magnetization. Theoretical work shows that these materials can even exhibit a large tunneling magnetoresistance [18], whereas the emergence of exotic phenomena such as the chiral anomaly [19] and magnetic spin Hall effect [20–23] makes them a very interesting playground for investigating the interplay of topology, electron transport, and magnetism [24–26].

A prime candidate of this material class is Mn_3Sn, a hexagonal Weyl metal in which the Mn atoms form kagome lattice planes stacked along the c axis with an inverse-triangular spin structure and all the spins oriented in plane [12,27–30]. The noncollinear antiferromagnetic order is best described by the magnetic octupole moment **g** of the six Mn spins that reside in two stacked inverted triangles on adjacent kagome layers [green arrow in Fig. 1(a)]. Magnetic anisotropy defines six possible orientations of the **g**-vector in the kagome plane [Fig. 1(b)]. The almost perfect 120° noncollinear spin alignment is slightly distorted by magnetic anisotropy, which leads to a weak ferromagnetic moment of approximately $0.002\mu_B$ per Mn atom in the direction of the **g**-vector. This conveniently allows for the manipulation of antiferromagnetic order by external magnetic fields, whereas the large AHE and anomalous Nernst effect (ANE) of Mn_3Sn provide direct information on the orientation of **g** [31–34]. Importantly for applications, the topological properties of Mn_3Sn emerge in both polycrystalline and epitaxial thin films [33–40].

Pioneering work on Mn_3Sn/heavy metal bilayers has demonstrated switching of antiferromagnetic order by current-induced spin-orbit torques [41–44]. In these experiments, a change of the AHE as a function of current

*krishnag@mat.ethz.ch

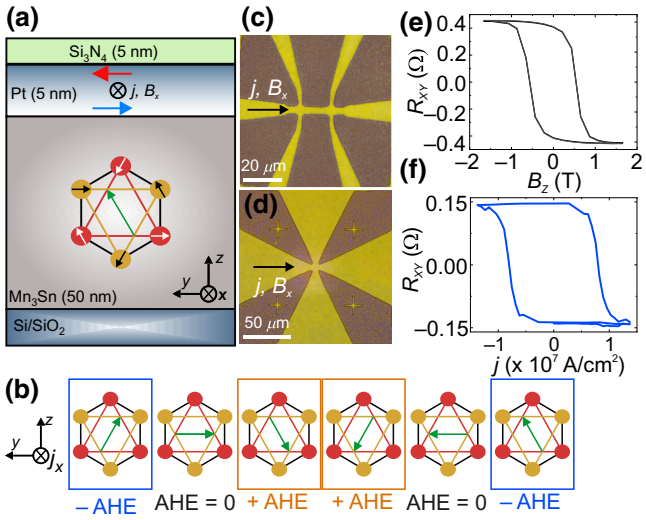

FIG. 1. (a) Cross section of the Mn_3Sn/Pt bilayer. The inverted triangular spin structure is shown in the center: white and black arrows represent the Mn spins and the green arrow the octupole vector **g**. (b) Possible orientations of **g** and corresponding AHE signal. Microscope images of (c) Hall bar device and (d) Hall cross used for switching and time-resolved measurements. AHE of Mn_3Sn/Pt as a function of (e) magnetic field along z and (f) current density for $10-\mu$s-long pulses and $B_x = +200$ mT.

reveals the reorientation of **g** in crystal grains with the c axis oriented in plane. Switching only occurs in the presence of a symmetry-breaking magnetic field collinear with the current, with the final state determined by the relative orientation of current and field and by the sign of the spin Hall angle in the heavy metal [41,42,45]. These observations suggest a switching mechanism very similar to that of ferromagnet/heavy metal bilayers [7,46,47]. Within this picture, however, different magnetization dynamics can be expected depending on whether the torques rotate the moments in or out of the kagome plane [41,43,48,49]. Other effects such as chiral spin rotation have been proposed, whereby the Mn moments undergo continuous rotation in the kagome plane with time periods in the tens of nanoseconds [43,48,50]. Thus far, however, switching experiments have relied on electrical pulses with a pulse duration of 100 ms, which yield no information about the fast switching dynamics expected of antiferromagnets.

In this work, we explore the chiral switching dynamics of Mn_3Sn/Pt bilayers. We observe that the switching behavior varies characteristically with the pulse length and shape: conventional bistable switching between $\pm z$ states is observed for pulses with fall times longer than 400 ns whereas tristable switching is observed for pulses with shorter fall times, leading to a demagnetized state with zero AHE. By studying the switching dependence on the temporal shape of the pulses, applied field, temperature, and time we show that the reversal of the **g**-vector occurs through two phases, namely current-induced partial demagnetization lasting several nanoseconds followed by cooling in the presence of spin-orbit torques at the end of a current pulse. This mechanism is similar to the setting of exchange bias during field cooling in coupled antiferromagnetic-ferromagnetic systems [51]. However, it differs from the thermally activated switching observed in collinear ferromagnets [52] and antiferromagnets [3], in which Joule heating reduces the magnetic anisotropy energy barrier while the sample remains magnetic. Time-resolved measurements during pulsing indicate that the reversal of chiral antiferromagnetic order is incoherent and that chiral spin rotation is either damped or averaged out in polycrystalline Mn_3Sn. Our measurements also set a limit on the reversal speed attainable by the interplay of current-induced heating and spin-orbit torques in chiral antiferromagnets.

II. METHODS

Our samples are polycrystalline Mn_3Sn(50 nm)/Pt(5 nm) bilayers grown by magnetron sputtering patterned into 3- to 6-μm-wide Hall bars and Hall crosses [Figs. 1(c) and 1(d)] [53]. High-resolution transmission electron microscopy reveals the presence of columnar grains of about 250 nm in width, different orientations, and excellent crystalline order [53]. Measurements of the longitudinal resistance (R_{xx}) and transverse Hall resistance (R_{xy}) are consistent with previous work on similar samples [14,41,42,45,50,53]. We use a quasistatic pulse-probe protocol for characterizing the switching properties as a function of pulse shape and field [46] and perform time-resolved measurements of the AHE using the split-pulse technique described in Ref. [54]. In the pulse-probe method we inject a current pulse of up to 20 mA to induce switching followed by an alternate current of 1 mA, which allows for probing the first- and second-harmonic contributions to R_{xy} that are proportional to the AHE and ANE, respectively [53,55]. In the time-resolved measurements, we probe the change in AHE during a current pulse with a temporal resolution of about 50 ps [54]. Hall bars are used for quasistatic switching and Hall crosses for the time-resolved measurements. Given the structure of our samples, the AHE (ANE) reflects the out-of-plane (in-plane) component of **g** averaged over different crystal grains in the region sensed by the Hall resistance [31,35,38,53]. Comparative switching measurements on Mn_3Sn/W and W/Mn_3Sn/Pt samples are reported in Ref. [53].

III. RESULTS

A. Multistate switching determined by the pulse fall time

Figures 1(e) and 1(f) show the field- and current-induced switching of the **g**-vector, respectively, as measured by the AHE. In agreement with previous reports [35,41,42], we

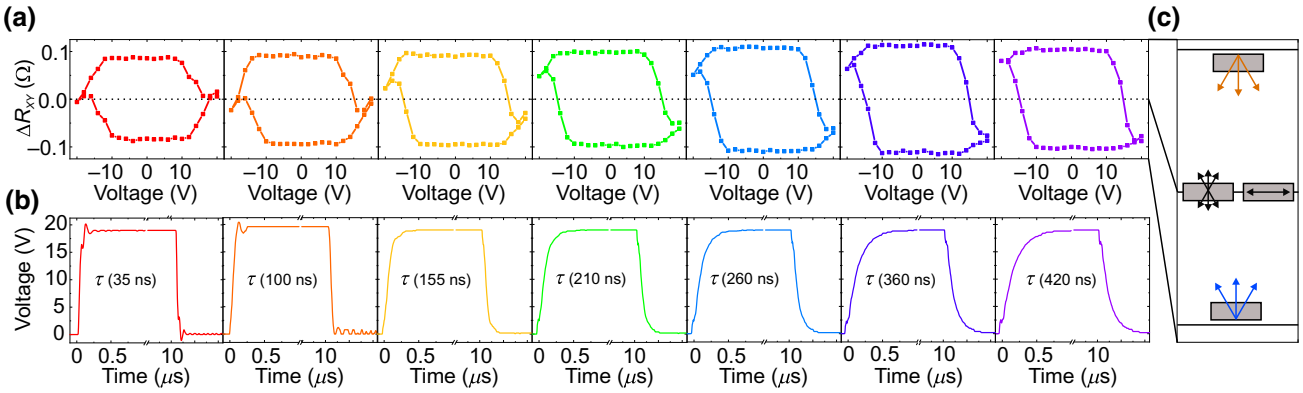

FIG. 2. (a) Switching loops of Mn_3Sn/Pt as a function of pulse voltage with rise and fall time increasing from left to right. (b) Corresponding pulse shape. (c) Schematic showing the $-z$, $+z$, and intermediate states and the possible orientations of the **g**-vector in each state.

observe switching of about 30% of the total AHE upon injecting 10-μs-long current pulses with a fall time $\tau =$ 420 ns. This bistable behavior is interpreted as **g** switching between the $+z$ and $-z$ states. Surprisingly, however, we find that gradually reducing τ to below 100 ns changes the switching from bistable to tristable, leading to the appearance of states with high and low AHE at intermediate current values and zero AHE at high current (Fig. 2). Because the pulse length is constant, the gradual shift of the endpoint R_{xy} in Fig. 2(a) demonstrates that the fall time determines the switching regime. Importantly, the magnetic state set by the current pulse and magnetic field remains constant after the pulse. The occurrence of multistate switching has been reported before in Mn_3Sn [43], but the role of the transient dynamic effects that determine the final orientation of the **g**-vector has not been elucidated. These effects can be of two types: thermal due to Joule heating and magnetic due to spin-orbit torques.

B. Switching as a function of in-plane field

To exclude a purely thermal origin of the switching, we study its dependence on the external in-plane magnetic field B_x. Figures 3(a) and 3(b) show the current-induced switching loops for 10-μs-long pulses with $\tau = 35$ and 420 ns, respectively, for increasing values of B_x. The reversal of the switching direction upon inversion of B_x indicates that switching is due to spin-orbit torques in the entire range of fall times. We also find that the switching amplitude between $+z$ and $-z$ states, $\Delta R_{xy} = R_{xy}(2\text{ V}) - R_{xy}(-2\text{ V})$, increases up to $B_x \approx 100$ mT, consistent with previous reports [35,41–43,45] and the standard model of spin-orbit torque switching in ferromagnets [7,46]. However, ΔR_{xy} decreases in the high-field limit [black squares in Figs. 3(c) and 3(d)], indicating that another mechanism comes into play. We also note that the offset of R_{xy} and the sign of the switching amplitude ΔR_{xy} (± 20 V) in the short-pulse regime are very sensitive to the presence of an out-of-plane external field [53].

C. Switching by current-induced heating and cooling in the presence of spin-orbit torques

To understand the role played by heating we measure the AHE as a function of temperature [Figs. 4(a) and 4(b)]. The AHE vanishes at $T_N = 390$ K, close to the Néel

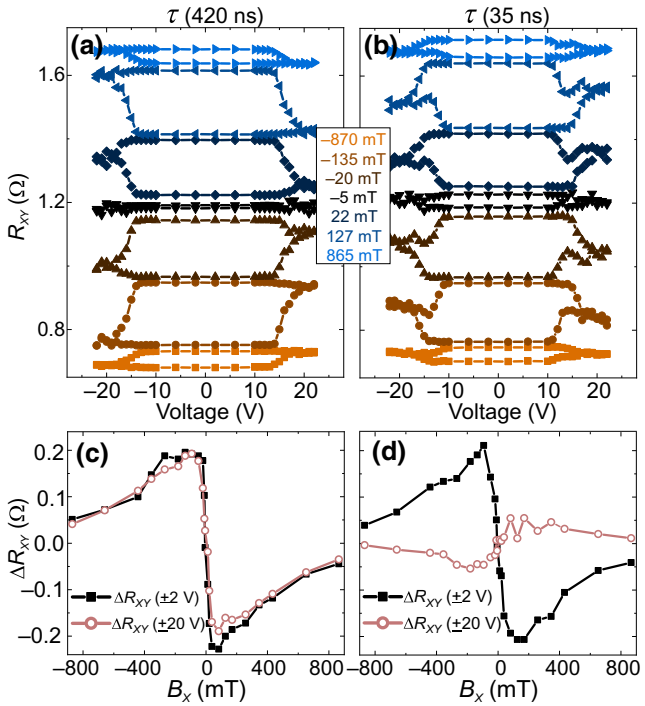

FIG. 3. Field dependence of the current-induced switching for (a) long- and (b) short-fall-time pulses of 10 μs in length. Switching amplitude ΔR_{xy} between ± 2 V (black squares) and ± 20 V (purple circles) as a function of B_x for (c) long and (d) short fall time.

temperature of bulk Mn_3Sn (420 K) [30,43]. The longitudinal resistance R_{xx} has a nonlinear temperature behavior as it is a mixture of the resistance due to Pt and Mn_3Sn. Measuring R_{xx} as a function of current allows us to gauge the extent of Joule heating, which shows that the sample temperature reaches T_N for pulse currents larger than 14 mA (16 V) [53]. We thus propose a model to explain the multistate switching behavior in which the interplay of temperature and spin-orbit torques is governed by τ. Consider a generic voltage pulse that heats up the sample and provides a current density j to exert a torque, as shown in Fig. 4(c). As the pulse starts, the temperature increases quadratically with the current at a rate determined by the longest between the pulse rise time and the heat diffusion time. For pulses longer than a few tens of nanoseconds, the sample temperature approaches T_N, leading to a demagnetized state until cooling down begins at the end of the pulse. Deterministic switching to a final state $+z$ or $-z$ can be achieved only if j is larger than a critical current density j_c as the temperature has dropped below T_N, i.e., for long τ. If, on the other hand, the current drops abruptly below j_c when the temperature is still close to T_N, the Mn_3Sn grains freeze in a mixed multidomain configuration, which leads to an intermediate state with no AHE for short τ. Our simultaneous measurements of the AHE and ANE show that this intermediate state consists of domains along $\pm z$, which give a net zero AHE, and grains that are oriented along $+x$ and $-x$ for $B_x > 0$ and $B_x < 0$, respectively [53]. The fraction of grains oriented along $\pm x$ during cooling down increases with B_x, which explains the nonmonotonic field dependence of the switching amplitude in Fig. 3. Thus, by gradually modifying τ, we tune the fraction of grains that switch and those that remain demagnetized at the end of the pulse.

This model also explains why the $\pm z$ final states with large/low AHE can be reached starting from the intermediate state with zero AHE upon reducing the pulse voltage in small incremental steps, as seen in Fig. 2 even for short τ. Figure 4(d) shows R_{xy} recorded by sweeping the pulse amplitude from $+18$ to -18 V and back in steps of 2 V (black dots). Starting from the intermediate state obtained by pulsing at $+18$ V with $\tau = 35$ ns, the AHE changes progressively to the low state upon reducing the pulse amplitude. However, if the pulse amplitude is abruptly decreased from $+18$ to $+10$ V, no switching occurs (green dots). The type of switching thus depends on the initial state and on the decrement step size, which is different from the change of switching amplitude as a function of current reported for bistable switching in Ref. [41]. Our observation is consistent with different Mn_3Sn grains having a distribution of T_N due to their varying sizes, which are selectively switched to the $\pm z$ final states upon decreasing the pulse amplitude from the intermediate state. This is essentially a stepwise version of the long-fall-time scenario described above.

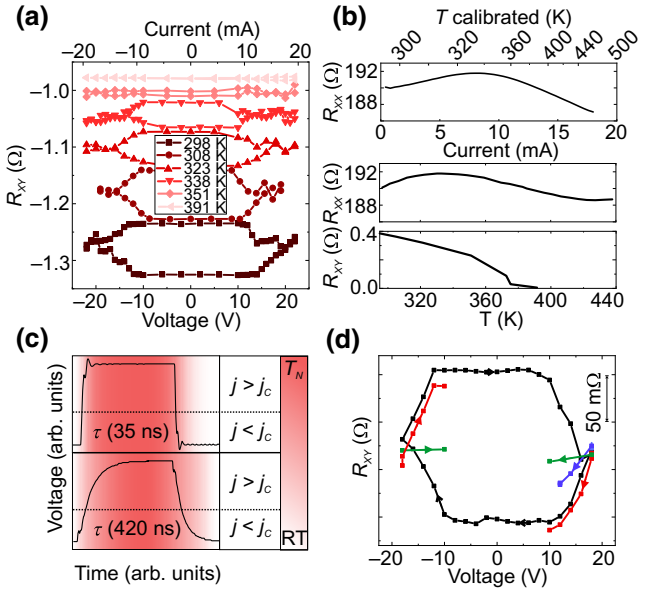

FIG. 4. (a) AHE switching as a function of pulse voltage at different temperatures for 10-μs-long pulses. (b) Temperature dependence of R_{xy} (bottom panel) and R_{xx} (middle panel) of Mn_3Sn/Pt. R_{xx} versus direct current and calibrated temperature (top panel). (c) Schematic current pulse with temperature profile indicated by the red shading. (d) Stepwise switching sequences: R_{xy} versus pulse amplitude starting from ± 18 V in steps of 2 V (black, red), 4 V (blue), and 8 V (green).

Overall, our results show that the switching of antiferromagnetic order in Mn_3Sn occurs due to heat-assisted demagnetization followed by reorientation of the **g**-vector induced by spin-orbit torques during cooling down. The fall time of the current pulses determines the final magnetic configuration of the Mn_3Sn domains. Additionally, switching loops measured for 21-V pulses of decreasing length, from 50 to 5 ns, evidence that the switching amplitude vanishes in the limit of short pulses [Fig. 5(a)]. These findings show that switching of antiferromagnetic order in Mn_3Sn by spin-orbit torques has a composite temporal dependence and different dynamics relative to ferromagnets [54,56] and collinear antiferromagnets [3,57,58].

D. Time-resolved measurements

To determine the transient dynamics, we perform time-resolved measurements of R_{xy} during the current pulses using the setup shown in Fig. 5(b). The temporal evolution of the AHE voltage V_H during the switching process is determined by taking the difference of the Hall voltage trace measured during switching relative to a reference trace in the absence of switching [54]. Figure 5(c) shows the average of 20 differential time traces of V_H taken during pulses with $+21$-V amplitude, 75-ns duration and $\tau = 0.3$ ns, separated by a 1-s delay. The decrease (increase) of V_H following the onset of the pulse at $t = 0$ for $B_x = +250$

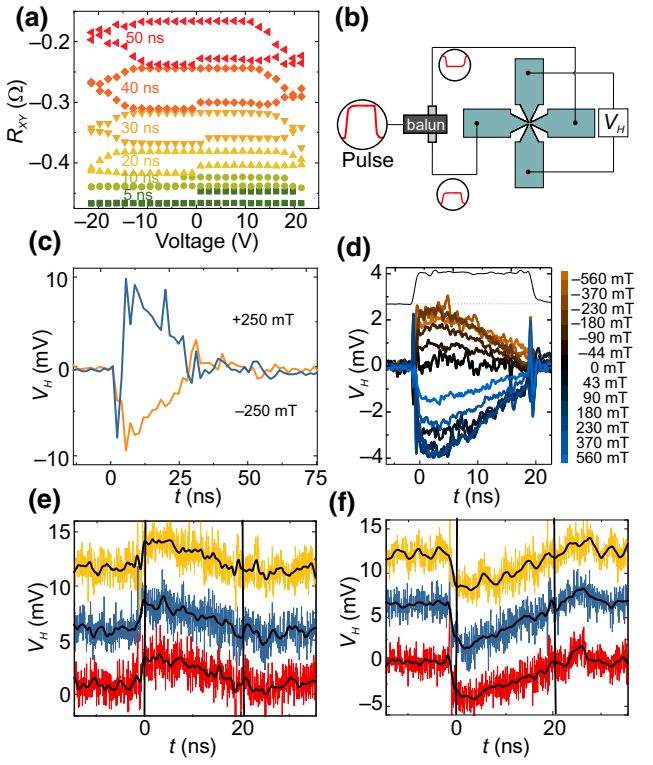

FIG. 5. (a) Current-induced switching loops for different pulse lengths, $\tau = 0.3$ ns, and $B_x = -250$ mT. (b) Schematic of the time-resolved AHE measurements. (c) Differential switching time traces averaged over 20 consecutive +21-V pulses with $B_x = \pm 250$ mT. The pulses are 75-ns long starting at $t = 0$. (d) Differential switching time traces averaged over 100 consecutive 20-ns-long voltage pulses of amplitude +21 V versus B_x. The gray trace at the top shows the pulse shape. Single-shot differential switching traces for 20-ns-long voltage pulses at (e) $B_x = -180$ mT and (f) $B_x = +180$ mT. The black lines are moving averages over 1.5 ns.

mT (−250 mT) reflects the decrease (increase) of the AHE from the initial $-z$ ($+z$) state to the intermediate state with no AHE. It takes about 35 ns for $|V_H|$ to reduce to 0, after which no further changes of V_H are observed until the end of the pulse. Measurements performed for 20-ns-long pulses as a function of B_x, reported in Fig. 5(d), further reveal that the amplitude of the transient switching signal scales with B_x and that the timescale over which $|V_H|$ reduces to 0 is independent of B_x. We thus associate the decrease of $|V_H|$ with the time it takes for the device to reach a temperature close to T_N, in line with the switching mechanism proposed above. This time depends only on j and not on B_x, which shows that the switching speed of Mn_3Sn is ultimately limited by the heating rate.

Recent studies propose a coherent chiral spin-reversal mechanism in noncollinear antiferromagnets where the **g**-vector continuously rotates above a given current density threshold [43,48,50]. The rotation period is estimated in a range of 1–30 ns, depending on the current density. Indirect evidence for this effect has been reported for both epitaxial and polycrystalline thin films [43,50].

The experimental evidence for such a mechanism, however, lacks insight into the time-dependent dynamics that is the hallmark of coherent switching. Our time-resolved traces shown in Figs. 5(c) and 5(d) evidence a monotonic decrease of $|V_H|$ that is not consistent with reproducible oscillations of R_{xy} due to chiral spin rotation. Because these traces are averaged over several pulses, they do not provide information on stochastic rotations. To investigate the occurrence of chiral spin rotation during individual current pulses, we thus measure single-shot time traces of V_H. Representative examples of such traces are shown in Figs. 5(e) and 5(f) for a series of 20-ns-long current pulses. Our analysis does not reveal evidence of periodic oscillations of V_H consistent with chiral spin rotation during single-shot pulses.

The absence of oscillations can be ascribed to various factors. First, chiral spin rotation requires an injected spin current with polarization parallel to the c axis [43]. Given the polycrystalline nature of our samples, we estimate having a measurable amount of such grains in our Hall crosses [43,50,53]. On the other hand, chiral spin rotation may take place in different grains with different phase factors, averaging to zero in the total Hall signal. According to simulations, however, these coherent effects should result in visible oscillations also in polycrystalline samples [50]. Another possibility is that the rotation is too fast to be resolved by our measurements, which have a temporal resolution of about 50 ps [54]. The current density in the time-resolved measurements is 1.3×10^7 A/cm^2 when averaged over the entire thickness of Mn_3Sn/Pt and about 6.2×10^7 A/cm^2 in Pt, as estimated using a parallel resistor model. The rotation frequency corresponding to this current is 1.7 GHz [43], which is within our time resolution. The continuous decrease of the AHE signal thus indicates that any oscillation, if present, is strongly damped and that heat-induced demagnetization dominates over coherent effects.

IV. CONCLUSIONS

In summary, our work shows that the switching of chiral antiferromagnetic order in Mn_3Sn/Pt is incoherent and determined by the timed interplay of heat and spin-orbit torques. Both effects are current-induced ones but heating up to T_N occurs on a timescale of tens of nanoseconds whereas the injection of a spin current from Pt closely follows the temporal profile of the current pulses. Switching proceeds via a two-step demagnetization-remagnetization process, whereby the final orientation of the **g**-vector is deterministic between $\pm z$ states only if the sample cools down in the presence of a spin current larger than a critical value. Our results provide insight into the switching timescale and dynamics of topological antiferromagnets,

showing that it is different from that of both ferromagnets and collinear antiferromagnets and limited by the sample heating rate. Additionally, this work shows that time-resolved Hall effect measurements provide a viable method to investigate the current-induced dynamics of antiferromagnetic order in topological materials.

ACKNOWLEDGMENTS

This research is partially supported by the Swiss National Science Foundation (Grants No. 200020-200465 and No. PZ00P2-179944). During the resubmission of the manuscript we became aware of related work reporting the multistate switching of Mn_3Sn [59].

[1] P. Wadley, *et al.*, Spintronics: Electrical switching of an antiferromagnet, Science **351**, 587 (2016).

[2] K. Olejník, V. Schuler, X. Marti, V. Novák, Z. Kašpar, P. Wadley, R. P. Campion, K. W. Edmonds, B. L. Gallagher, J. Garces, M. Baumgartner, P. Gambardella, and T. Jungwirth, Antiferromagnetic CuMnAs multi-level memory cell with microelectronic compatibility, Nat. Commun. **8**, 15434 (2017).

[3] M. Meinert, D. Graulich, and T. Matalla-Wagner, Electrical Switching of Antiferromagnetic Mn_2Au and the Role of Thermal Activation, Phys. Rev. Appl. **9**, 064040 (2018).

[4] S. DuttaGupta, A. Kurenkov, O. A. Tretiakov, G. Krishnaswamy, G. Sala, V. Krizakova, F. Maccherozzi, S. S. Dhesi, P. Gambardella, S. Fukami, and H. Ohno, Spin-orbit torque switching of an antiferromagnetic metallic heterostructure, Nat. Commun. **11**, 5715 (2020).

[5] S. A. Siddiqui, J. Sklenar, K. Kang, M. J. Gilbert, A. Schleife, N. Mason, and A. Hoffmann, Metallic antiferromagnets, J. Appl. Phys. **128**, 040904 (2020).

[6] S. Arpaci, V. Lopez-Dominguez, J. Shi, L. Sánchez-Tejerina, F. Garesci, C. Wang, X. Yan, V. K. Sangwan, M. A. Grayson, M. C. Hersam, G. Finocchio, and P. Khalili Amiri, Observation of current-induced switching in non-collinear antiferromagnetic $IrMn_3$ by differential voltage measurements, Nat. Commun. **12**, 3828 (2021).

[7] A. Manchon, J. Železný, I. M. Miron, T. Jungwirth, J. Sinova, A. Thiaville, K. Garello, and P. Gambardella, Current-induced spin-orbit torques in ferromagnetic and antiferromagnetic systems, Rev. Mod. Phys. **91**, 035004 (2019).

[8] X. Marti, I. Fina, C. Frontera, J. Liu, P. Wadley, Q. He, R. J. Paull, J. D. Clarkson, J. Kudrnovský, I. Turek, J. Kuneš, D. Yi, J.-H. Chu, C. T. Nelson, L. You, E. Arenholz, S. Salahuddin, J. Fontcuberta, T. Jungwirth, and R. Ramesh, Room-temperature antiferromagnetic memory resistor, Nat. Mater. **13**, 367 (2014).

[9] C. C. Chiang, S. Y. Huang, D. Qu, P. H. Wu, and C. L. Chien, Absence of Evidence of Electrical Switching of the Antiferromagnetic Néel Vector, Phys. Rev. Lett. **123**, 227203 (2019).

[10] B. J. Jacot, G. Krishnaswamy, G. Sala, C. O. Avci, S. Vélez, P. Gambardella, and C.-H. Lambert, Systematic study of nonmagnetic resistance changes due to electrical pulsing in single metal layers and metal/antiferromagnet bilayers, J. Appl. Phys. **128**, 173902 (2020).

[11] T. Matalla-Wagner, J.-M. Schmalhorst, G. Reiss, N. Tamura, and M. Meinert, Resistive contribution in electrical-switching experiments with antiferromagnets, Phys. Rev. Res. **2**, 033077 (2020).

[12] S. Nakatsuji, N. Kiyohara, and T. Higo, Large anomalous Hall effect in a non-collinear antiferromagnet at room temperature, Nature **527**, 212 (2015).

[13] A. K. Nayak, J. E. Fischer, Y. Sun, B. Yan, J. Karel, A. C. Komarek, C. Shekhar, N. Kumar, W. Schnelle, J. Kübler, C. Felser, and S. S. P. Parkin, Large anomalous Hall effect driven by a nonvanishing Berry curvature in the noncolinear antiferromagnet Mn_3Ge, Sci. Adv. **2**, e1501870 (2016).

[14] T. Higo, D. Qu, Y. Li, C. L. Chien, Y. Otani, and S. Nakatsuji, Anomalous Hall effect in thin films of the Weyl antiferromagnet Mn_3Sn, Appl. Phys. Lett. **113**, 1 (2018).

[15] A. L. Balk, N. H. Sung, S. M. Thomas, P. F. Rosa, R. D. McDonald, J. D. Thompson, E. D. Bauer, F. Ronning, and S. A. Crooker, Comparing the anomalous Hall effect and the magneto-optical Kerr effect through antiferromagnetic phase transitions in Mn_3Sn, Appl. Phys. Lett. **114**, 032401 (2019).

[16] H. C. Zhao, H. Xia, S. Hu, Y. Y. Lv, Z. R. Zhao, J. He, E. Liang, G. Ni, L. Y. Chen, X. P. Qiu, S. M. Zhou, and H. B. Zhao, Large ultrafast-modulated Voigt effect in non-collinear antiferromagnet Mn_3Sn, Nat. Commun. **12**, 5266 (2021).

[17] T. Uchimura, J.-Y. Yoon, Y. Sato, Y. Takeuchi, S. Kanai, R. Takechi, K. Kishi, Y. Yamane, S. DuttaGupta, J. Ieda, H. Ohno, and S. Fukami, Observation of domain structure in non-collinear antiferromagnetic Mn_3Sn thin films by magneto-optical Kerr effect, Appl. Phys. Lett. **120**, 172405 (2022).

[18] J. Dong, X. Li, G. Gurung, M. Zhu, P. Zhang, F. Zheng, E. Y. Tsymbal, and J. Zhang, Tunneling magnetoresistance in noncollinear antiferromagnetic tunnel junctions, ArXiv:2112.06568 (2021).

[19] K. Kuroda, *et al.*, Evidence for magnetic Weyl fermions in a correlated metal, Nat. Mater. **16**, 1090 (2017).

[20] M. Kimata, H. Chen, K. Kondou, S. Sugimoto, P. K. Muduli, M. Ikhlas, Y. Omori, T. Tomita, A. H. MacDonald, S. Nakatsuji, and Y. Otani, Magnetic and magnetic inverse spin Hall effects in a non-collinear antiferromagnet, Nature **565**, 627 (2019).

[21] K. Kondou, H. Chen, T. Tomita, M. Ikhlas, T. Higo, A. H. MacDonald, S. Nakatsuji, and Y. Otani, Giant field-like torque by the out-of-plane magnetic spin Hall effect in a topological antiferromagnet, Nat. Commun. **12**, 6491 (2021).

[22] S. Hu, D.-F. Shao, H. Yang, M. Tang, Y. Yang, W. Fan, S. Zhou, E. Y. Tsymbal, and X. Qiu, Efficient field-free perpendicular magnetization switching by a magnetic spin Hall effect, ArXiv:2103.09011 (2021).

[23] S. Ghosh, A. Manchon, and J. Železný, Unconventional Robust Spin-Transfer Torque in Noncollinear Antiferromagnetic Junctions, Phys. Rev. Lett. **128**, 097702 (2022).

[24] E. V. Gomonay and V. M. Loktev, Spintronics of antiferromagnetic systems, Low Temp. Phys. **40**, 17 (2014).

[25] V. Baltz, A. Manchon, M. Tsoi, T. Moriyama, T. Ono, and Y. Tserkovnyak, Antiferromagnetic spintronics, Rev. Mod. Phys. **90**, 015005 (2018).

[26] L. Šmejkal, Y. Mokrousov, B. Yan, and A. H. MacDonald, Topological antiferromagnetic spintronics, Nat. Phys. **14**, 242 (2018).

[27] S. Tomiyoshi and Y. Yamaguchi, Magnetic structure and weak ferromagnetism of Mn_3Sn studied by polarized neutron diffraction, J. Phys. Soc. Jpn. **51**, 2478 (1982).

[28] H. Ohmori, S. Tomiyoshi, H. Yamauchi, and H. Yamamoto, Spin structure and weak ferromagnetism of Mn_3Sn, J. Magn. Magn. Mater. **70**, 249 (1987).

[29] T. F. Duan, W. J. Ren, W. L. Liu, S. J. Li, W. Liu, and Z. D. Zhang, Magnetic anisotropy of single-crystalline Mn_3Sn in triangular and helix-phase states, Appl. Phys. Lett. **107**, 082403 (2015).

[30] Y. Song, Y. Hao, S. Wang, J. Zhang, Q. Huang, X. Xing, and J. Chen, Complicated magnetic structure and its strong correlation with the anomalous Hall effect in Mn_3Sn, Phys. Rev. B **101**, 144422 (2020).

[31] M. Ikhlas, T. Tomita, T. Koretsune, M. T. Suzuki, D. Nishio-Hamane, R. Arita, Y. Otani, and S. Nakatsuji, Large anomalous Nernst effect at room temperature in a chiral antiferromagnet, Nat. Phys. **13**, 1085 (2017).

[32] X. Li, L. Xu, L. Ding, J. Wang, M. Shen, X. Lu, Z. Zhu, and K. Behnia, Anomalous Nernst and Righi-Leduc Effects in Mn_3Sn: Berry Curvature and Entropy Flow, Phys. Rev. Lett. **119**, 056601 (2017).

[33] T. Ikeda, M. Tsunoda, M. Oogane, S. Oh, T. Morita, and Y. Ando, Fabrication and evaluation of highly c-plane oriented Mn_3Sn thin films, AIP Adv. **10**, 015310 (2020).

[34] T. Nakano, T. Higo, A. Kobayashi, S. Miwa, S. Nakatsuji, and K. Yakushiji, Fabrication of polycrystalline Weyl antiferromagnetic Mn_3Sn thin films on various seed layers, Phys. Rev. Mater. **5**, 054402 (2021).

[35] T. Higo, H. Man, D. B. Gopman, L. Wu, T. Koretsune, O. M. J. V. Erve, Y. P. Kabanov, D. Rees, Y. Li, M.-t. Suzuki, S. Patankar, M. Ikhlas, C. L. Chien, R. Arita, R. D. Shull, J. Orenstein, and S. Nakatsuji, Large magneto-optical Kerr effect and imaging of magnetic octupole domains in an antiferromagnetic metal, Nat. Photonics **12**, 73 (2018).

[36] T. Ikeda, M. Tsunoda, M. Oogane, S. Oh, T. Morita, and Y. Ando, Improvement of large anomalous Hall effect in polycrystalline antiferromagnetic $Mn_{3+x}Sn$ thin films, IEEE Trans. Magn. **55**, 1 (2019).

[37] Y. You, X. Chen, X. Zhou, Y. Gu, R. Zhang, F. Pan, and C. Song, Anomalous Hall effect-like behavior with in-plane magnetic field in noncollinear antiferromagnetic Mn_3Sn Films, Adv. Electron. Mater. **5**, 1800818 (2019).

[38] J. Yoon, Y. Takeuchi, R. Itoh, S. Kanai, S. Fukami, and H. Ohno, Crystal orientation and anomalous Hall effect of sputter-deposited non-collinear antiferromagnetic Mn_3Sn thin films, Appl. Phys. Express **13**, 013001 (2020).

[39] J.-Y. Yoon, Y. Takeuchi, S. DuttaGupta, Y. Yamane, S. Kanai, J. Ieda, H. Ohno, and S. Fukami, Correlation of anomalous Hall effect with structural parameters and magnetic ordering in $Mn_{3+x}Sn_{1-x}$ thin films, AIP Adv. **11**, 065318 (2021).

[40] D. Khadka, T. R. Thapaliya, S. Hurtado Parra, X. Han, J. Wen, R. F. Need, P. Khanal, W. Wang, J. Zang, J. M. Kikkawa, L. Wu, and S. X. Huang, Kondo physics in antiferromagnetic Weyl semimetal $Mn_{3+x}Sn_{1-x}$ films, Sci. Adv. **6**, eabc1977 (2020).

[41] H. Tsai, T. Higo, K. Kondou, T. Nomoto, A. Sakai, A. Kobayashi, T. Nakano, K. Yakushiji, R. Arita, S. Miwa, Y. Otani, and S. Nakatsuji, Electrical manipulation of a topological antiferromagnetic state, Nature **580**, 608 (2020).

[42] H. Tsai, T. Higo, K. Kondou, A. Kobayashi, T. Nakano, K. Yakushiji, S. Miwa, Y. Otani, and S. Nakatsuji, Spin–orbit torque switching of the antiferromagnetic state in polycrystalline Mn_3Sn/Cu/heavy metal heterostructures, AIP Adv. **11**, 045110 (2021).

[43] Y. Takeuchi, Y. Yamane, J. Y. Yoon, R. Itoh, B. Jinnai, S. Kanai, J. Ieda, S. Fukami, and H. Ohno, Chiral-spin rotation of non-collinear antiferromagnet by spin–orbit torque, Nat. Mater. **20**, 1364 (2021).

[44] Y. Deng, R. Li, and X. Liu, Thickness dependent anomalous Hall effect in noncollinear antiferromagnetic Mn_3Sn polycrystalline thin films, J. Alloys Compd. **874**, 159910 (2021).

[45] H. Tsai, T. Higo, K. Kondou, S. Sakamoto, A. Kobayashi, T. Matsuo, S. Miwa, Y. Otani, and S. Nakatsuji, Large Hall signal due to electrical switching of an antiferromagnetic Weyl semimetal state, Small Sci. **1**, 2000025 (2021).

[46] I. M. Miron, K. Garello, G. Gaudin, P.-J. Zermatten, M. V. Costache, S. Auffret, S. Bandiera, B. Rodmacq, A. Schuhl, and P. Gambardella, Perpendicular switching of a single ferromagnetic layer induced by in-plane current injection, Nature **476**, 189 (2011).

[47] M. Baumgartner, K. Garello, J. Mendil, C. O. Avci, E. Grimaldi, C. Murer, J. Feng, M. Gabureac, C. Stamm, Y. Acremann, S. Finizio, S. Wintz, J. Raabe, and P. Gambardella, Spatially and time-resolved magnetization dynamics driven by spin–orbit torques, Nat. Nanotechnol. **12**, 980 (2017).

[48] H. Fujita, Field-free, spin-current control of magnetization in non-collinear chiral antiferromagnets, Phys. Status Solidi (RRL) **11**, 1600360 (2017).

[49] Y. Yamane, O. Gomonay, and J. Sinova, Dynamics of noncollinear antiferromagnetic textures driven by spin current injection, Phys. Rev. B **100**, 054415 (2019).

[50] G. Q. Yan, S. Li, H. Lu, M. Huang, Y. Xiao, L. Wernert, J. A. Brock, E. E. Fullerton, H. Chen, H. Wang, and C. R. Du, Quantum sensing and imaging of spin–orbit-torque-driven spin dynamics in the non-collinear antiferromagnet Mn_3Sn, Adv. Mater. **34**, 2200327 (2022).

[51] J. Nogués and I. K. Schuller, Exchange bias, J. Magn. Magn. Mater. **192**, 203 (1999).

[52] E. Grimaldi, V. Krizakova, G. Sala, F. Yasin, S. Couet, G. Sankar Kar, K. Garello, and P. Gambardella, Single-shot dynamics of spin–orbit torque and spin transfer torque switching in three-terminal magnetic tunnel junctions, Nat. Nanotechnol. **15**, 111 (2020).

[53] See Supplemental Material at http://link.aps.org/supplemental/10.1103/PhysRevApplied.18.024064 for details of the sample fabrication, crystal structure, time-resolved measurements, switching of Mn_3Sn/W and W/Mn_3Sn/Pt,

temperature calibration, orientation of domains probed by the ANE, and dependence of the switching amplitude on applied field.

[54] G. Sala, V. Krizakova, E. Grimaldi, C. H. Lambert, T. Devolder, and P. Gambardella, Real-time Hall-effect detection of current-induced magnetization dynamics in ferrimagnets, Nat. Commun. **12**, 656 (2021).

[55] C. O. Avci, K. Garello, M. Gabureac, A. Ghosh, A. Fuhrer, S. F. Alvarado, and P. Gambardella, Interplay of spin-orbit torque and thermoelectric effects in ferromagnet/normal-metal bilayers, Phys. Rev. B **90**, 224427 (2014).

[56] V. Krizakova, E. Grimaldi, K. Garello, G. Sala, S. Couet, G. S. Kar, and P. Gambardella, Interplay of Voltage Control of Magnetic Anisotropy, Spin-Transfer Torque, and Heat in the Spin-Orbit-Torque Switching of Three-Terminal Magnetic Tunnel Junctions, Phys. Rev. Appl. **15**, 054055 (2021).

[57] M. S. Wörnle, P. Welter, Z. Kašpar, K. Olejník, V. Novák, R. P. Campion, P. Wadley, T. Jungwirth, C. L. Degen, and P. Gambardella, Current-induced fragmentation of antiferromagnetic domains, ArXiv:1912.05287 (2019).

[58] Z. Kašpar, M. Surýnek, J. Zubáč, F. Krizek, V. Novák, R. P. Campion, M. S. Wörnle, P. Gambardella, X. Marti, P. Němec, K. W. Edmonds, S. Reimers, O. J. Amin, F. Maccherozzi, S. S. Dhesi, P. Wadley, J. Wunderlich, K. Olejník, and T. Jungwirth, Quenching of an antiferromagnet into high resistivity states using electrical or ultrashort optical pulses, Nat. Electron. **4**, 30 (2021).

[59] B. Pal, B. K. Hazra, B. Göbel, J.-C. Jeon, A. K. Pandeya, A. Chakraborty, O. Busch, A. K. Srivastava, H. Deniz, J. M. Taylor, H. Meyerheim, I. Mertig, S.-H. Yang, and S. S. P. Parkin, Setting of the magnetic structure of chiral kagome antiferromagnets by a seeded spin-orbit torque, Sci. Adv. **8**, eabo5930 (2022).